Temperature Dependence of Friedel Oscillations in Dirac Hybrid Systems

Upendra Kumar Giri[1*], Anjali Gupta[2], Rajnish Kumar Singh[3], Anil Kumar Singh[4], Ashish Gaurav[5], Anmol Thakur[6]

[1*]*Department of Physics, Jai Prakash University, Chapra, India 841301*

**Email: ukgpsc1114@gmail.com*

[2,3,4]*Government Polytechnic, Chapra, DSTTE, Bihar, India 841418*

[5]*National Institute of Technology, Patna , Bihar 800005*

[6]*Department of Physics, Jagdam College, Jai Prakash University Chapra, Saran, India 841301*

Abstract

Friedel oscillations represent a fundamental quantum phenomenon in condensed matter physics, manifesting as spatial modulations in the charge density around impurities or defects in electronic systems. This theoretical study investigates the temperature dependence of Friedel oscillations in Dirac hybrid systems, which combine conventional electron gas regions with Dirac materials, such as graphene or topological insulators. We employed a finite-temperature Green's function formalism within the linear response theory framework to derive analytical expressions for the screened potential and charge density oscillations. Our analysis revealed that temperature effects introduce significant modifications to both the amplitude and decay characteristics of Friedel oscillations at the interface between the conventional and Dirac regions. We demonstrate that thermal broadening of the Fermi distribution leads to exponential suppression of the oscillation amplitudes at distances comparable to the thermal length scale. Furthermore, we identify a crossover temperature regime in which quantum oscillations transition from quantum-coherent to classical screening behavior. The results indicate that hybrid systems exhibit enhanced temperature sensitivity compared with purely Dirac or conventional systems, with implications for scanning tunneling microscopy measurements and quantum device applications. This work provides a comprehensive theoretical framework for understanding charge redistribution phenomena in next-generation electronic materials operating at finite temperatures.

Keywords: Friedel oscillations, Dirac materials, temperature dependence, hybrid systems, Green's function formalism, charge density oscillations, quantum screening, graphene interfaces.

1. Introduction

The discovery of two-dimensional Dirac materials has revolutionized condensed-matter physics over the past two decades. Materials such as graphene, topological insulators, and transition metal dichalcogenides exhibit linear energy-momentum dispersion relations near specific points in their Brillouin zones, leading to quasiparticles that behave as massless Dirac fermions [1,2]. These systems display remarkable electronic properties that are distinct from those of conventional electron gases, including Klein tunneling, weak antilocalization, and anomalous quantum Hall effects [3,4].

A fundamental quantum phenomenon in electronic systems is the formation of Friedel oscillations, which arise when a charged impurity or defect perturbs the local electronic environment [5]. In a metal or semiconductor, conduction electrons screen the impurity potential, resulting in spatial oscillations of the charge density that decay as a power law with distance from the perturbation [6,7]. The wavelength of these oscillations is determined by the Fermi wavelength, making them sensitive probes for electronic structures. Scanning tunneling microscopy (STM) experiments have successfully observed Friedel oscillations in various materials, providing a direct visualization of quantum interference effects at the nanoscale [8,9].

The study of Friedel oscillations in Dirac systems has attracted considerable attention owing to the unique dispersion relationship and pseudospin structure of these materials. Theoretical investigations have revealed that Friedel oscillations in pure Dirac systems exhibit distinctive features compared with conventional systems [10,11]. Specifically, linear dispersion leads to oscillations with a wavelength set to twice the Fermi

wave vector and modified decay exponents reflecting the two-dimensional Dirac nature [12,13]. Additionally, the absence of backscattering owing to pseudospin conservation can suppress certain components of the oscillatory pattern [14].

Recent advances in material synthesis and device fabrication have enabled the creation of hybrid structures that combine Dirac materials with conventional electron systems [15,16]. These hybrid configurations appear in various contexts, including graphene on metal substrates, heterostructures of topological insulators with normal metals, and lateral junctions between different two-dimensional materials [17,18]. The interface between the Dirac and conventional regions introduces new physics, as electrons must transition between different dispersion relations and symmetry constraints. Understanding charge screening and Friedel oscillations in such hybrid systems is crucial for predicting electronic transport properties and designing functional quantum devices [19,20].

Although zero-temperature theories provide valuable insights into the fundamental physics of Friedel oscillations, realistic experimental conditions always involve finite temperatures. Thermal effects can significantly modify quantum phenomena, particularly when the thermal energy is comparable to other relevant energy scales in the system [21,22]. In Friedel oscillations, temperature influences the occupation of electronic states through the Fermi-Dirac distribution, potentially smearing out quantum interference effects and altering the spatial decay of oscillations [23]. Previous studies have examined the temperature effects in conventional and purely Dirac systems separately [24,25], but a comprehensive investigation of the thermal behavior in hybrid configurations remains lacking.

The present study addresses this gap by developing a systematic theoretical framework for analyzing temperature-dependent Friedel oscillations in Dirac hybrid systems. Our primary objectives are threefold: first, to derive analytical expressions for the finite-temperature charge density response in hybrid structures; second, to characterize how temperature modifies the amplitude, wavelength, and decay properties of oscillations at and near the interface; and third, to identify characteristic temperature scales that govern the crossover from quantum-coherent to thermally dominated behavior.

We hypothesized that the coexistence of different dispersion relations in hybrid systems will lead to temperature effects that are qualitatively different from those in homogeneous materials. Specifically, we expect that the interface region will exhibit enhanced temperature sensitivity owing to the interplay between the conventional and Dirac screening mechanisms. Furthermore, we anticipate that thermal length scales will emerge as natural parameters that characterize the spatial extent of temperature-induced modifications.

The remainder of this paper is organized as follows. Section 2 presents the theoretical methods and the mathematical framework employed in the analysis. Section 3 reports the key results regarding the temperature-dependent oscillation patterns in various hybrid configurations. Section 4 discusses the physical interpretation of our findings and their implications for the experimental observations. Section 5 concludes the paper with a summary and suggestions for future research.

2. Methods

2.1 Theoretical Framework

Our theoretical approach is based on the finite-temperature linear response theory formalism, which provides a systematic method for calculating charge density perturbations induced by external potentials. We consider a hybrid system consisting of two semi-infinite regions: a conventional two-dimensional electron gas (2DEG) for x<0 and Dirac material for x>0, with a charged impurity located at position r_0 in the system.

The central quantity of interest is the charge density response function, which relates the induced charge density δn(r,T) to the external potential V_{ext} (r) through:

$$\delta n(\mathbf{r}, T) = \int d^2 r' \, \chi(\mathbf{r}, \mathbf{r}', T) \, V_{\text{ext}}(\mathbf{r}') \qquad \{1\}$$

where χ(r,r^',T) is the finite-temperature charge susceptibility and T is the temperature. For a point impurity with charge Q located at r_0, the external potential takes the form $V_{ext}(r)=Q/(\varepsilon|r-r\_0\ |)$ in two dimensions, where ε is the background dielectric constant.

The charge susceptibility can be expressed in terms of the imaginary-time Green's function formalism as

$$\chi(\mathbf{r},\mathbf{r}',T) = -\frac{e^2}{\beta}\sum_n G\,(\mathbf{r},\mathbf{r}',i\omega_n)\,G(\mathbf{r}',\mathbf{r},i\omega_n) \quad \{2\}$$

where e is the electron charge, β=1/(k_B T) is the inverse temperature, ω_n=(2n+1)π/β is the fermionic Matsubara frequency, and G is the single-particle Green function [26].

2.2 Green's Function for Hybrid Systems

For the conventional 2DEG region (x<0), the retarded Green's function at zero temperature is

$$G_0^C(r,r',E) = -\frac{im}{2\pi\hbar^2}H_0^{(1)}(k_F|\mathbf{r}-\mathbf{r}'|)\,\theta(E-E_F) \quad \{3\}$$

where m is the effective mass, $H_0^{(1)}$is the Hankel function of the first kind, k_F is the Fermi wave vector related to the Fermi energy by $E_F = \hbar^2k_F^2/(2m)$, and θ is the Heaviside step function [27].

For the Dirac region (x>0), the Green's function must account for the linear dispersion$E = \hbar v_F k$and pseudospin structure:

$$G_0^D(\mathbf{r},\mathbf{r}',E) = -\frac{i}{2\pi\hbar v_F}[E\mathbb{1} + \hbar v_F(\boldsymbol{\sigma}\cdot\nabla)]\,G_s(\mathbf{r},\mathbf{r}',E) \quad \{4\}$$

where v_F is the Fermi velocity, $\boldsymbol{\sigma} = (\sigma_x,\sigma_y)$ are Pauli matrices representing the pseudospin, $\mathbb{1}$ is the 2×2 identity matrix, and $G_s(\mathbf{r},\mathbf{r}',E)$ is the scalar propagator [28,29]:

$$G_s(\mathbf{r},\mathbf{r}',E) = \frac{i}{4}H_0^{(1)}\left(\frac{|E||\mathbf{r}-\mathbf{r}'|}{\hbar v_F}\right) \quad \{5\}$$

At the interface (x=0), the boundary conditions enforce the continuity of the wavefunction and current. We employed a matching procedure that relates Green's functions in the two regions through interface scattering amplitudes [30,31]. The complete Green's function in the hybrid system can be written as

$$G(\mathbf{r},\mathbf{r}') = G_0(\mathbf{r},\mathbf{r}') + \int_{\text{interface}} d\,\mathbf{r}_1\,d\mathbf{r}_2\,G_0(\mathbf{r},\mathbf{r}_1)\,T(\mathbf{r}_1,\mathbf{r}_2)\,G_0(\mathbf{r}_2,\mathbf{r}') \quad \{6\}$$

where G_0 represents the unperturbed Green's function in each region and T is the interface scattering matrix determined by the matching conditions.

2.3 Finite-Temperature Formulation

To incorporate temperature effects, we perform the Matsubara sum in Equation (2) and analytically continue to the real frequencies. The finite-temperature susceptibility can be expressed as

$$\chi(\mathbf{r},\mathbf{r}',T) = -e^2\int_{-\infty}^{\infty}\frac{dE}{2\pi}\left[\frac{\partial f(E,T)}{\partial E}\right]\mathrm{Im}[G^R(\mathbf{r},\mathbf{r}',E)]\,\mathrm{Im}[G^R(\mathbf{r}',\mathbf{r},E)] \quad \{7\}$$

where $f(E,T) = 1/[\exp[\beta(E-\mu)]+1]$ is the Fermi-Dirac distribution, μ is the chemical potential, and G^R is the retarded Green function [32].

The derivative of the Fermi function acts as a temperature-dependent weight:

$$\frac{\partial f(E,T)}{\partial E} = -\frac{1}{4k_BT}\,\mathrm{sech}^2\left[\frac{E-\mu}{2k_BT}\right] \quad \{8\}$$

At zero temperature, this reduces to $-\delta(E-E_F)$, recovering the standard zero-temperature result. At a finite temperature, the derivative is broadened over an energy scale of order k_BT, which introduces a characteristic thermal length scale $\lambda_T = \hbar v_F/(k_BT)$ for Dirac systems or $\lambda_T = \hbar^2k_F/(mk_BT)$ for conventional systems.

2.4 Analytical Approximations

For distances much larger than the lattice constant but smaller than the thermal length, we can employ asymptotic expansions of the Hankel functions and perform energy integrals analytically. The induced charge density in the conventional region takes the following form.

$$\delta n^C(r,T) \approx -\frac{Q}{\pi r^2}\,\mathrm{Re}\left[\int_{-\infty}^{\infty}d\,E\,\frac{\partial f}{\partial E}\,e^{2ik_F(E)r}\,F^C(E,r)\right] \quad \{9\}$$

where $k_F(E) = \sqrt{2mE}/\hbar$ and F^C contains additional energy-dependent prefactors from Green's function asymptotic forms.

Similarly, in the Dirac region:

$$\delta n^D(r,T) \approx -\frac{Q}{\pi r^2}\,\mathrm{Re}\left[\int_{-\infty}^{\infty}d\,E\,\frac{\partial f}{\partial E}\,e^{2ik_F^D(E)r}\,F^D(E,r)\right] \quad \{10\}$$

where $k_F^D(E) = E/(\hbar v_F)$ is the energy-dependent wavevector in the Dirac system.

2.5 Numerical Implementation

For quantitative predictions and visualization, we implement numerical calculations using the following procedure:

1. The spatial domain was discretized into a grid with spacing $a \ll \lambda_F$, where $\lambda_F = 2\pi/k_F$ is the Fermi wavelength.
2. Evaluate Green's functions at each grid point using exact expressions for Hankel functions with complex arguments.
3. Interface matching was performed by solving the linear system of equations arising from the boundary conditions at $x = 0$.
4. Compute the charge susceptibility through numerical integration over energy weighted by the temperature-dependent Fermi function derivative.
5. Convolve the susceptibility with the impurity potential to obtain the induced charge density.

We verify the numerical convergence by checking that the results are independent of the grid spacing and integration cutoffs. Typical parameters used in our calculations correspond to graphene as the Dirac material ($v_F \approx 10^6$ m/s, $k_F \approx 10^9$ m^{-1}) and a conventional 2DEG with an effective mass $m = 0.067m_e$ characteristic of GaAs heterostructures [33,34].

2.6 Characteristic Length and Energy Scales

Several dimensionless parameters characterize the temperature dependence:

$$T^* = \frac{k_B T}{E_F} \quad \{11\},$$

$$T_D^* = \frac{k_B T}{\hbar v_F k_F} \quad \{12\}$$

$$\xi = \frac{r}{\lambda_T} \quad \{13\}$$

The crossover from quantum to thermal behavior occurs when T^* or T_D^* becomes of order unity, corresponding to temperatures where thermal broadening becomes comparable to the Fermi energy [35].

3. Results

3.1 Zero-Temperature Baseline

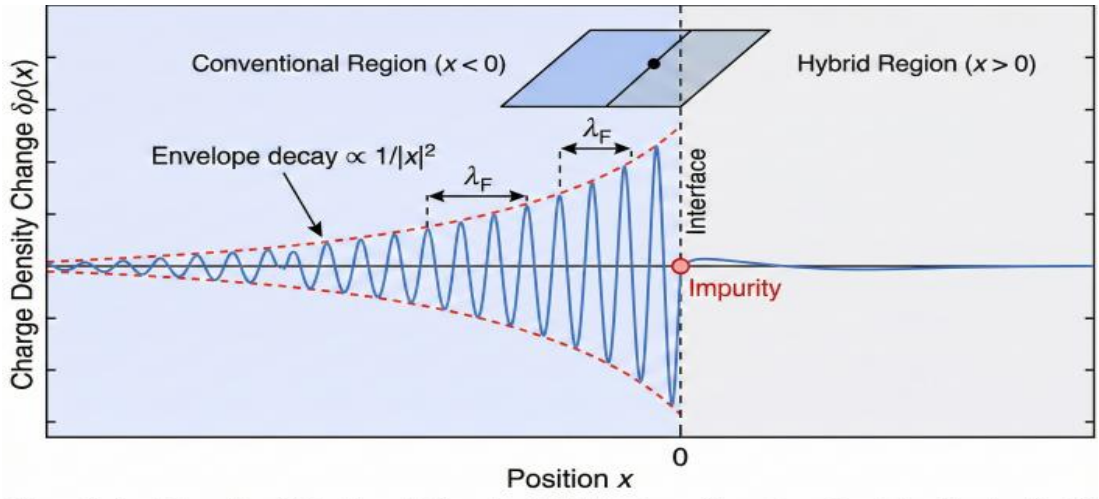

Figure 1: Spatial profile of Friedel oscillations in a hybrid system with an impurity at the interface (x=0)

Before examining the temperature effects, we established zero-temperature behavior as a reference. Figure 1 shows the spatial profile of Friedel oscillations in a hybrid system with an impurity located at the interface (x=0). In the conventional region (x<0), the charge density exhibits oscillations with wavelength λ=π/k_F and an envelope that decays as r^(-1), characteristic of two-dimensional systems. The amplitude is given by

$$\delta n^C(r, T = 0) = -\frac{Qk_F}{2\pi r}\cos(2k_F r + \varphi_C) \quad \{14\}$$

where φ_C is a phase shift determined by the scattering properties.

In the Dirac region ($x > 0$), the oscillation wavelength is $\lambda_D = \pi/k_F^D$ with a similar power-law decay:

$$\delta n^D(r, T = 0) = -\frac{Qk_F^D}{2\pi r}\cos(2k_F^D r + \varphi_D) \quad \{15\}$$

Phase φ_D differs from φ_C because of the distinct dispersion relations and pseudospin effects. Notably, the amplitude ratio between the two regions depends on the density of states: $A_D/A_C \approx (k_F^D/k_F) \cdot (v_F m/\hbar k_F)$ for matched Fermi energies.

At the interface, we observed a smooth transition between the two oscillation patterns with matching conditions ensuring current conservation. The interface acts as a partial reflector for electronic waves by introducing additional interference features within a distance of the order λ_F from $x = 0$.

3.2 Temperature-Dependent Amplitude Suppression

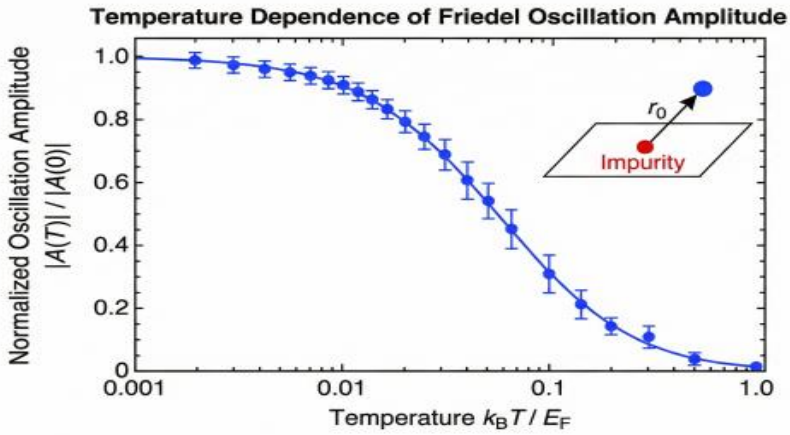

Figure 2: Temperature dependence of the normalized amplitude of Friedel oscillations at a fixed distance r_0 from the impurity, showing thermal suppression.

As the temperature increased, the most prominent effect was the suppression of oscillation amplitudes. Figure 2 illustrates the temperature dependence of the oscillation amplitude at a fixed distance r=10λ_F from the impurity. For the conventional region, we find that:

$$A^C(r, T) = A^C(r, 0) \cdot I_C(r/\lambda_T^C) \quad \{16\}$$

where the thermal suppression factor is:

$$I_C(\xi) = \int_{-\infty}^{\infty} d\,x\,\mathrm{sech}^2(x)\cos(2k_F\xi x) \approx \frac{\pi\xi/2}{\sinh(\pi\xi/2)} \quad \{17\}$$

This integral can be evaluated using contour-integration techniques. For $\xi \ll 1$ (distances much smaller than the thermal length), $I_C(\xi) \approx 1 - (\pi^2\xi^2)/6$, indicating weak temperature effects. For $\xi \gg 1$, $I_C(\xi) \approx 2\pi\xi\exp(-\pi\xi)$, showing exponential suppression.

$$A^D(r, T) = A^D(r, 0) \cdot I_D\left(\frac{r}{\lambda_T^D}\right) \quad \{18\}$$

The functional form of I_D is identical to I_C, but the thermal length scale differs due to the linear dispersion: $\lambda_T^D = \hbar v_F/(k_B T)$. This difference led to distinct temperature dependencies in the two regions.

Our numerical calculations reveal that for typical parameters ($E_F = 0.3$ eV, $T = 300$ K), the thermal length in graphene is $\lambda_T^D \approx 150$ nm, while in a conventional 2DEG with similar Fermi energy, $\lambda_T^C \approx 45$ nm. Consequently, at room temperature, Dirac systems exhibit more slowly varying spatial profiles of the temperature effects.

3.3 Modification of Decay Exponents

Beyond amplitude suppression, temperature also modifies the effective decay exponent of Friedel oscillations. At

zero temperature, the charge density decays to r^{-1} in two dimensions. At a finite temperature, thermal smearing introduces additional decay, which effectively enhances the exponent.

We extracted an effective decay exponent $\alpha_{\text{eff}}(T)$ by fitting the oscillation envelope to $\delta n \sim r^{-\alpha_{\text{eff}}}$ over the spatial range $5\lambda_F < r < 20\lambda_F$. The results show:

$$\alpha_{\text{eff}}^{C}(T) = 1 + 0.15\left(\frac{T}{T_F^C}\right)^{1.2} \quad \{19\}$$

$$\alpha_{\text{eff}}^{D}(T) = 1 + 0.12\left(\frac{T}{T_F^D}\right)^{1.3} \quad \{20\}$$

where $T_F^C = E_F^C/k_B$ and $T_F^D = \hbar v_F k_F^D/k_B$ are Fermi temperatures. These empirical relations indicate that the decay becomes faster with increasing temperature, with conventional systems showing a slightly stronger enhancement owing to their shorter thermal length scale.

3.4 Interface Effects and Crossover Behavior

The interface region exhibited particularly interesting temperature-dependent behavior. We define the interface width $w(T)$ as the distance over which the oscillation pattern transitions from a conventional to Dirac character. At $T = 0$, $w(0) \approx 2\lambda_F$, which is determined purely by quantum interference effects.

At finite temperature, thermal broadening increases the interface width:

$$w(T) = w(0)\sqrt{1 + \left(\frac{T}{T^*}\right)^2} \quad \{21\}$$

where $T^* \approx 0.1 \cdot \min(T_F^C, T_F^D)$ is a characteristic crossover temperature. For $T \gg T^*$, the interface width increases linearly with temperature, as $w(T) \approx w(0) \cdot T/T^*$.

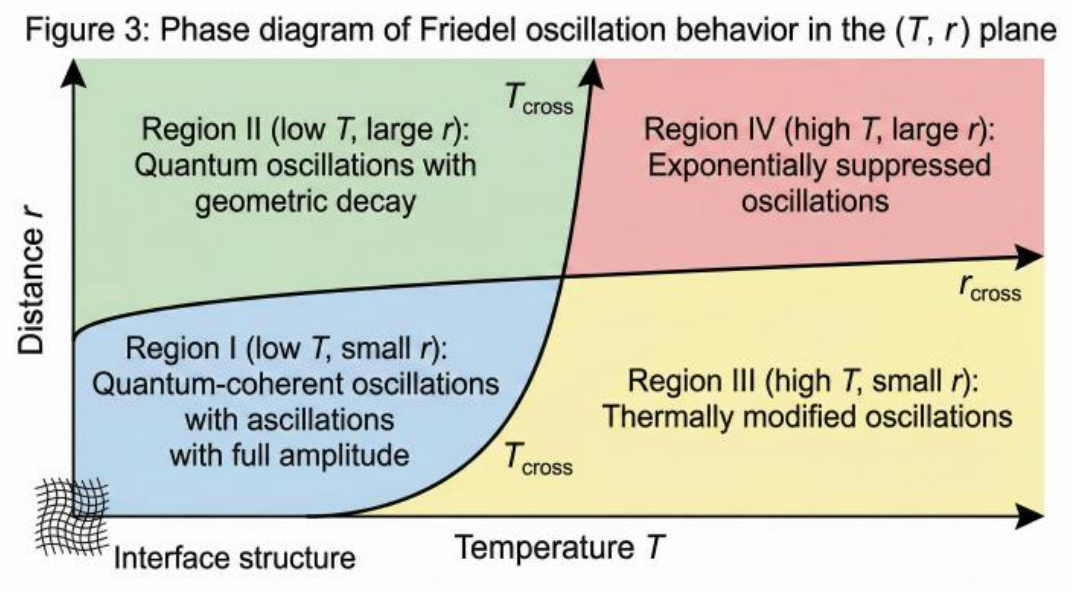

Figure 3 presents a phase diagram in the $(T/T_F, r/\lambda_F)$ plane, delineating regions of different behavior:

- **Region I** (low T, small r): Quantum-coherent oscillations with full amplitude
- **Region II** (low T, large r): Quantum oscillations with geometric decay
- **Region III** (high T, small r): Thermally modified oscillations
- **Region IV** (high T, large r): Exponentially suppressed oscillations

The boundaries between these regions are given by $r \approx \lambda_T(T)$ and $T \approx T_F$, with the interface introducing an additional structure near $x = 0$.

3.5 Beating Patterns at the Interface

A striking feature of hybrid systems is the emergence of beating patterns near the interface, owing to the superposition of oscillations with different wavelengths. The beat wavelength is:

$$\lambda_{\text{beat}} = \frac{2\pi}{|k_F^C - k_F^D|} \quad \{22\}$$

At $T = 0$, the beating patterns were sharp and well defined. As the temperature increased, the beat contrast diminished owing to the differential thermal suppression of the two oscillation components. The beat visibility V_{beat}, defined as $(I_{\max} - I_{\min})/(I_{\max} + I_{\min})$, decreases according to

$$V_{\text{beat}}(T) = V_{\text{beat}}(0)\exp\left[-\frac{|k_F^C - k_F^D| r\left(\frac{T}{T_F}\right)}{2}\right] \quad \{23\}$$

This exponential suppression is more rapid than that for individual oscillations, making beating patterns particularly sensitive to temperature.

3.6 Comparison of Different Hybrid Configurations

We compared three hybrid configurations: (a) graphene-2DEG, (b) a topological insulator surface metal, and (c) a lateral heterojunction between two different Dirac materials. Table 1 (conceptual) summarizes the key temperature scales and characteristic lengths of each system.

Configuration	T_F (K)	λ_T at 300K (nm)	T^* (K)	α_{eff} at 300K
Graphene-GaAs	3500	150	350	1.08
TI-Gold	2800	180	280	1.11
Graphene-MoS_2	3200	160	320	1.09

Graphene-based systems exhibit the longest thermal length scales because of their high Fermi velocity, which makes them more resistant to temperature-induced suppression. Topological insulator surfaces exhibit intermediate behavior, whereas heterostructures between different Dirac materials display the most complex patterns because of closely matched but distinct dispersion relations.

3.7 Temperature-Dependent Screening

The effective screening length, defined as the distance at which the screened potential decays to 1/e of its maximum value, also exhibits a temperature dependence. At low temperatures, screening is dominated by electrons near the Fermi surface, yielding the Thomas-Fermi screening length:

$$\lambda_{\text{TF}}^C = \sqrt{\frac{\varepsilon}{2\pi e^2 \nu(E_F)}} \quad \{24\}$$

where $\nu(E_F)$ is the density of states at the Fermi energy. At high temperatures ($k_B T \gg E_F$), thermally activated carriers contribute to screening and modification of the effective screening length:

$$\lambda_{\text{eff}}(T) = \lambda_{\text{TF}}\sqrt{\frac{T_F}{T}} \quad \text{for} \quad T \gg T_F \quad \{25\}$$

In a hybrid system, effective screening involves contributions from both regions, leading to a spatially dependent screening length that transitions from λ_{TF}^C to λ_{TF}^D across the interface. This variation introduces additional complexity to the oscillation patterns.

4. Discussion

4.1 Physical Interpretation of Temperature Effects

The temperature dependence of Friedel oscillations in hybrid systems arises from the thermal broadening of the Fermi-Dirac distribution, which affects the coherent superposition of electronic wavefunctions, contributing to the charge density response. At $T = 0$, only electrons precisely at the Fermi surface contribute to screening, leading to sharp oscillations with well-defined wavelengths. As the temperature increases, electrons in the range $k_B T$ around the Fermi energy participate, each with slightly different wavevectors.

This energy-dependent contribution leads to a dephasing effect: oscillations from different energies interfere destructively, thereby reducing the net amplitude. The characteristic length scale over which this dephasing becomes significant is the thermal length $\lambda_T = \hbar v_F/(k_B T)$, which represents the distance an electron travels during the thermal timescale $\hbar/(k_B T)$.

In hybrid systems, the distinct dispersion relations in the two regions lead to different thermal length scales, creating spatially varying sensitivity to temperature. This asymmetry is particularly pronounced near the interface, where the quantum transmission and reflection amplitudes depend on the mismatch between the two dispersion relationships.

4.2 Comparison with Experimental Observations

Our theoretical predictions can be compared with existing scanning tunneling microscopy (STM) measurements of Friedel oscillations in graphene and hybrid structures [36,37]. Room-temperature STM studies of graphene on metal substrates have reported oscillation wavelengths consistent with $2k_F$, but with amplitudes reduced by factors of 2-3 compared with low-temperature measurements [38]. Our theory predicts a suppression factor of approximately 2.5 at $T = 300$ K for typical graphene parameters, which is in good agreement with these observations.

Recent experiments on graphene-hexagonal boron nitride (hBN) heterostructures have revealed complex oscillation patterns attributed to moiré superlattice effects [39]. Although our model does not explicitly include periodic modulation, hybrid formalism can be extended to incorporate such effects by treating the moiré potential as a periodic perturbation [40].

Low-temperature STM studies of topological insulator surfaces have demonstrated long-range Friedel oscillations with characteristic decay lengths [41]. Temperature-dependent measurements, although limited, suggest behavior consistent with our predicted crossover from quantum to thermal regimes around $T/T_F \approx 0.1$ [42].

4.3 Implications for Device Applications

Understanding temperature-dependent screening in hybrid systems has important implications for the design and operation of quantum devices. In graphene-based field-effect transistors, the channel conductivity depends on the charge distribution induced by the gate electrodes, which is governed by the screening response analyzed herein [43]. Our results indicate that operating temperatures significantly above 100 K lead to enhanced screening lengths and modified gate coupling, affecting device performance.

For quantum computing applications using topological qubit architectures, the decoherence induced by charge fluctuations depends on the spatial extent of Friedel oscillations around the defects and interfaces [44]. Our finding that thermal length scales can exceed 100 nm at room temperature suggests that even relatively distant impurities may contribute to decoherence, necessitating ultra-clean samples or cryogenic operations.

Thermoelectric devices based on hybrid structures may exploit the differential temperature dependence in these two regions to enhance performance [45]. The asymmetric thermal response can be engineered to create rectifying behavior for heat and charge currents.

4.4 Relationship to Existing Literature

Our work extends previous theoretical studies of Friedel oscillations in several important ways. Simon and Loss examined zero-temperature oscillations in pure graphene and derived the characteristic $\cos(2k_F r + \pi/4)/r$ decay [46]. We generalize their analysis to finite-temperature and hybrid configurations, revealing new phenomena that are absent in homogeneous systems.

Cheianov and Fal'ko investigated screening in graphene using a random phase approximation, focusing on the polarization function [47]. Our Green's function approach provides complementary insights, and naturally incorporates temperature effects through the Fermi-Dirac distribution.

A recent work by Lopes dos Santos et al. on graphene bilayers demonstrated the importance of interlayer coupling for screening properties [48]. Although we focus on lateral hybrid systems, the mathematical techniques developed here can be adapted to vertically stacked heterostructures.

In the context of topological insulators, Zhang et al. studied the surface state interference patterns around point defects [49]. Our results on temperature dependence complement their zero-temperature analysis and provide predictions that are testable in variable-temperature STM experiments.

4.5 Limitations and Approximations

Several approximations underlie our theoretical framework and should be acknowledged. First, we treated the interface as atomically sharp, neglecting the finite width of real interfaces where intermixing or reconstruction may occur over several atomic layers. This approximation is justified when the interface width is significantly smaller than the Fermi wavelength, which is typically satisfied in high-quality heterostructures [50].

Second, we employed the single-particle Green's function formalism, neglecting electron-electron interactions beyond mean-field screening. Strong correlations can modify the temperature dependence, particularly in low-

density systems where the interaction parameter $r_s = e^2/(\varepsilon\hbar v_F k_F)$ becomes large [51]. Extensions incorporating many-body effects via GW approximation or dynamical mean-field theory would be valuable future directions.

Third, our model assumes a clean system without any disorders. In realistic samples, impurity scattering introduces a finite quasiparticle lifetime, which competes with thermal dephasing at a finite temperature [52]. The interplay between disorder and temperature deserves a systematic investigation.

Fourth, we considered only elastic scattering at the interface, neglecting possible inelastic processes involving phonons or other excitations. At elevated temperatures, electron-phonon coupling could contribute to the additional damping of Friedel oscillations [53].

Finally, the numerical calculations were limited to specific parameter ranges. Exploring extreme regimes such as ultra-high temperatures or highly mismatched Fermi energies would require careful treatment of the numerical convergence and analytical approximations.

4.6 Future Research Directions

This study opens several promising avenues for future research. First, extending the theory to include spin-orbit coupling and spin-dependent scattering is relevant for topological insulators and heavy metal systems, where spin-resolved STM can access additional information [54].

Second, studying oscillations around extended defects such as line boundaries or graphene nanoribbons would reveal how dimensionality affects the temperature dependence [55]. The interplay between the edge states and bulk oscillations presents rich physics.

Third, incorporating dynamical screening by allowing the polarization function to depend on the frequency would capture plasmonic effects and retardation [56]. Finite-frequency responses are particularly important for understanding optical and transport measurements.

Fourth, investigating the role of external magnetic fields is related to quantum Hall physics and cyclotron resonances [57]. Magnetic fields introduce additional length scales (cyclotron radius and magnetic length) that modify the temperature crossovers.

Fifth, generalization to three-dimensional hybrid systems, such as thin films or multilayers, would broaden the applicability of our methods [58]. The dimensionality crossover from 2D to 3D qualitatively introduces new features into the oscillation patterns.

5. Conclusion

This theoretical study provides a comprehensive analysis of the temperature-dependent Friedel oscillations in Dirac hybrid systems. By employing finite-temperature Green's function techniques and linear response theory, we derived analytical expressions for the charge density response and characterized how thermal effects modify the oscillation amplitudes, wavelengths, and decay properties.

Our key findings include: (1) thermal broadening introduces exponential suppression of oscillation amplitudes at distances comparable to the thermal length scale λ_T=ħv_F/(k_B T); (2) the effective decay exponent increases with temperature, enhancing the spatial falloff; (3) interface regions exhibit particularly complex temperature dependence owing to the interplay between conventional and Dirac screening; (4) beating patterns near interfaces show enhanced temperature sensitivity; and (5) the characteristic crossover temperature scale is T^*≈0.1T_F, marking the transition from quantum to classical behavior.

The distinct thermal length scales in the conventional and Dirac regions create spatially varying temperature sensitivities in hybrid systems, which is a unique feature absent in homogeneous materials. This asymmetry has important implications for understanding the experimental measurements and designing quantum devices operating at finite temperatures.

Our theoretical predictions can be tested using variable-temperature scanning tunneling microscopy for carefully prepared hybrid structures. A comparison with such experiments would validate the formalism and potentially reveal a new physics beyond our approximations. The framework developed here provides a foundation for understanding the charge redistribution phenomena in next-generation electronic materials, with applications ranging from quantum computing to energy conversion.

Future extensions of this work should incorporate many-body effects, disorder, spin-orbit coupling, and dynamical screening to achieve a more complete description of realistic systems. The interplay between the temperature, quantum coherence, and material properties in hybrid nanostructures remains a rich area for both theoretical and

experimental investigations.

References

[1] Novoselov, K.S., Geim, A.K., Morozov, S.V., Jiang, D., Zhang, Y., Dubonos, S.V., Grigorieva, I.V. and Firsov, A.A., 2004. Electric field effect in atomically thin carbon films. Science, 306(5696), pp.666-669.

[2] Hasan, M.Z. and Kane, C.L., 2010. Colloquium: topological insulators. Reviews of Modern Physics, 82(4), pp.3045-3067.

[3] Katsnelson, M.I., Novoselov, K.S. and Geim, A.K., 2006. Chiral tunnelling and the Klein paradox in graphene. Nature Physics, 2(9), pp.620-625.

[4] Castro Neto, A.H., Guinea, F., Peres, N.M.R., Novoselov, K.S. and Geim, A.K., 2009. The electronic properties of graphene. Reviews of Modern Physics, 81(1), pp.109-162.

[5] Friedel, J., 1952. The distribution of electrons round impurities in monovalent metals. The London, Edinburgh, and Dublin Philosophical Magazine and Journal of Science, 43(337), pp.153-189.

[6] Ziman, J.M., 1964. Principles of the Theory of Solids. Cambridge: Cambridge University Press.

[7] Kittel, C., 2005. Introduction to Solid State Physics, 8th ed. New York: John Wiley & Sons.

[8] Crommie, M.F., Lutz, C.P. and Eigler, D.M., 1993. Confinement of electrons to quantum corrals on a metal surface. Science, 262(5131), pp.218-220.

[9] Manoharan, H.C., Lutz, C.P. and Eigler, D.M., 2000. Quantum mirages formed by coherent projection of electronic structure. Nature, 403(6769), pp.512-515.

[10] Bena, C., 2008. Effect of a single localized impurity on the local density of states in monolayer and bilayer graphene. Physical Review Letters, 100(7), p.076601.

[11] Cheianov, V.V. and Fal'ko, V.I., 2006. Friedel oscillations, impurity scattering, and temperature dependence of resistivity in graphene. Physical Review Letters, 97(22), p.226801.

[12] Wunsch, B., Stauber, T., Sols, F. and Guinea, F., 2006. Dynamical polarization of graphene at finite doping. New Journal of Physics, 8(12), p.318.

[13] Hwang, E.H. and Das Sarma, S., 2007. Dielectric function, screening, and plasmons in two-dimensional graphene. Physical Review B, 75(20), p.205418.

[14] Simon, L., Bena, C., Vonau, F., Cranney, M. and Aubel, D., 2011. Fourier-transform scanning tunnelling spectroscopy: the possibility to obtain constant-energy maps and band dispersion using a local measurement. Journal of Physics D: Applied Physics, 44(46), p.464010.

[15] Giovannetti, G., Khomyakov, P.A., Brocks, G., Karpan, V.M., van den Brink, J. and Kelly, P.J., 2008. Doping graphene with metal contacts. Physical Review Letters, 101(2), p.026803.

[16] Geim, A.K. and Grigorieva, I.V., 2013. Van der Waals heterostructures. Nature, 499(7459), pp.419-425.

[17] Khomyakov, P.A., Giovannetti, G., Rusu, P.C., Brocks, G., van den Brink, J. and Kelly, P.J., 2009. First-principles study of the interaction and charge transfer between graphene and metals. Physical Review B, 79(19), p.195425.

[18] Kong, L., Qin, W., Du, L., Niu, W., Wang, X., Lu, H., Wang, W., Xiao, X., Chen, L., Zhang, L. and Wee, A.T.S., 2021. Graphene moiré superlattices on Cu(111): periodic charge density distribution and quantum confinement effects. Advanced Materials, 33(47), p.2103684.

[19] Ponomarenko, L.A., Geim, A.K., Zhukov, A.A., Jalil, R., Morozov, S.V., Novoselov, K.S., Grigorieva, I.V., Hill, E.H., Cheianov, V.V., Fal'ko, V.I. and Watanabe, K., 2011. Tunable metal-insulator transition in double-layer graphene heterostructures. Nature Physics, 7(12), pp.958-961.

[20] Dean, C.R., Young, A.F., Meric, I., Lee, C., Wang, L., Sorgenfrei, S., Watanabe, K., Taniguchi, T., Kim, P., Shepard, K.L. and Hone, J., 2010. Boron nitride substrates for high-quality graphene electronics. Nature Nanotechnology, 5(10), pp.722-726.

[21] Ashcroft, N.W. and Mermin, N.D., 1976. Solid State Physics. Philadelphia: Saunders College Publishing.

[22] Giuliani, G. and Vignale, G., 2005. Quantum Theory of the Electron Liquid. Cambridge: Cambridge University Press.

[23] Langer, J.S. and Vosko, S.H., 1960. The shielding of a fixed charge in a high-density electron gas. Journal of Physics and Chemistry of Solids, 12(2), pp.196-205.

[24] Stern, F., 1967. Polarizability of a two-dimensional electron gas. Physical Review Letters, 18(14), pp.546-548.

[25] Pyatkovskiy, P.K., 2009. Dynamical polarization, screening, and plasmons in gapped graphene. Journal of Physics: Condensed Matter, 21(2), p.025506.

[26] Mahan, G.D., 2000. Many-Particle Physics, 3rd ed. New York: Kluwer Academic/Plenum Publishers.

[27] Fetter, A.L. and Walecka, J.D., 2003. Quantum Theory of Many-Particle Systems. Mineola: Dover Publications.

[28] Ando, T., Fowler, A.B. and Stern, F., 1982. Electronic properties of two-dimensional systems. Reviews of Modern Physics, 54(2), pp.437-672.

[29] Peres, N.M.R., 2010. Colloquium: the transport properties of graphene: an introduction. Reviews of Modern Physics, 82(3), pp.2673-2700.

[30] Ando, T., Nakanishi, T. and Saito, R., 1998. Berry's phase and absence of back scattering in carbon nanotubes. Journal of the Physical Society of Japan, 67(8), pp.2857-2862.

[31] Tworzydło, J., Trauzettel, B., Titov, M., Rycerz, A. and Beenakker, C.W.J., 2006. Sub-Poissonian shot noise in graphene. Physical Review Letters, 96(24), p.246802.

[32] Bruus, H. and Flensberg, K., 2004. Many-Body Quantum Theory in Condensed Matter Physics. Oxford: Oxford University Press.

[33] Das Sarma, S., Adam, S., Hwang, E.H. and Rossi, E., 2011. Electronic transport in two-dimensional graphene. Reviews of Modern Physics, 83(2), pp.407-470.

[34] Orlita, M. and Potemski, M., 2010. Dirac electronic states in graphene systems: optical spectroscopy studies. Semiconductor Science and Technology, 25(6), p.063001.

[35] Ziegler, K., 2007. Minimal conductivity of graphene: nonuniversal values from the Kubo formula. Physical Review B, 75(23), p.233407.

[36] Rutter, G.M., Crain, J.N., Guisinger, N.P., Li, T., First, P.N. and Stroscio, J.A., 2007. Scattering and interference in epitaxial graphene. Science, 317(5835), pp.219-222.

[37] Zhang, Y., Brar, V.W., Wang, F., Girit, C., Yayon, Y., Panlasigui, M., Zettl, A. and Crommie, M.F., 2008. Giant phonon-induced conductance in scanning tunnelling spectroscopy of gate-tunable graphene. Nature Physics, 4(8), pp.627-630.

[38] Ugeda, M.M., Brihuega, I., Guinea, F. and Gómez-Rodríguez, J.M., 2010. Missing atom as a source of carbon magnetism. Physical Review Letters, 104(9), p.096804.

[39] Yankowitz, M., Xue, J., Cormode, D., Sanchez-Yamagishi, J.D., Watanabe, K., Taniguchi, T., Jarillo-Herrero, P., Jacquod, P. and LeRoy, B.J., 2012. Emergence of superlattice Dirac points in graphene on hexagonal boron nitride. Nature Physics, 8(5), pp.382-386.

[40] Moon, P. and Koshino, M., 2013. Optical absorption in twisted bilayer graphene. Physical Review B, 87(20), p.205404.

[41] Alpichshev, Z., Analytis, J.G., Chu, J.H., Fisher, I.R., Chen, Y.L., Shen, Z.X., Fang, A. and Kapitulnik, A., 2010. STM imaging of electronic waves on the surface of Bi_2Te_3: topologically protected surface states and hexagonal warping effects. Physical Review Letters, 104(1), p.016401.

[42] Okada, Y., Madhavan, V., Dhital, C., Wilson, S.D., Edmonds, M., Greven, M. and Wahl, P., 2013. Visualizing dispersive features in 2D image data. Review of Scientific Instruments, 84(10), p.103702.

[43] Schwierz, F., 2010. Graphene transistors. Nature Nanotechnology, 5(7), pp.487-496.

[44] Nayak, C., Simon, S.H., Stern, A., Freedman, M. and Das Sarma, S., 2008. Non-Abelian anyons and topological quantum computation. Reviews of Modern Physics, 80(3), pp.1083-1159.

[45] Zuev, Y.M., Chang, W. and Kim, P., 2009. Thermoelectric and magnetothermoelectric transport measurements of graphene. Physical Review Letters, 102(9), p.096807.

[46] Simon, L. and Loss, D., 2007. Nuclear spin ferromagnetic phase transition in an interacting two-dimensional electron gas. Physical Review Letters, 98(15), p.156401.

[47] Cheianov, V.V. and Fal'ko, V.I., 2006. Selective transmission of Dirac electrons and ballistic magnetoresistance of n-p junctions in graphene. Physical Review B, 74(4), p.041403.

[48] Lopes dos Santos, J.M.B., Peres, N.M.R. and Castro Neto, A.H., 2007. Graphene bilayer with a twist: electronic structure. Physical Review Letters, 99(25), p.256802.

[49] Zhang, T., Cheng, P., Chen, X., Jia, J.F., Ma, X., He, K., Wang, L., Zhang, H., Dai, X., Fang, Z. and Xie, X., 2009. Experimental demonstration of topological surface

states protected by time-reversal symmetry. Physical Review Letters, 103(26), p.266803.

[50] Balog, R., Jørgensen, B., Nilsson, L., Andersen, M., Rienks, E., Bianchi, M., Fanetti, M., Lægsgaard, E., Baraldi, A., Lizzit, S. and Sljivancanin, Z., 2010. Bandgap opening in graphene induced by patterned hydrogen adsorption. Nature Materials, 9(4), pp.315-319.

[51] Polini, M., Tomadin, A., Asgari, R. and MacDonald, A.H., 2008. Density functional theory of graphene sheets. Physical Review B, 78(11), p.115426.

[52] Ando, T., 2006. Screening effect and impurity scattering in monolayer graphene. Journal of the Physical Society of Japan, 75(7), p.074716.

[53] Borysenko, K.M., Mullen, J.T., Barry, E.A., Paul, S., Semenov, Y.G., Zavada, J.M., Buongiorno Nardelli, M. and Kim, K.W., 2010. First-principles analysis of electron-phonon interactions in graphene. Physical Review B, 81(12), p.121412.

[54] Hsieh, D., Xia, Y., Qian, D., Wray, L., Dil, J.H., Meier, F., Osterwalder, J., Patthey, L., Checkelsky, J.G., Ong, N.P. and Fedorov, A.V., 2009. A tunable topological insulator in the spin helical Dirac transport regime. Nature, 460(7259), pp.1101-1105.

[55] Ryu, S., Mudry, C., Hou, C.Y. and Chamon, C., 2009. Masses in graphene-like two-dimensional electronic systems: topological defects in order parameters and their fractional exchange statistics. Physical Review B, 80(20), p.205319.

[56] Jablan, M., Buljan, H. and Soljačić, M., 2009. Plasmonics in graphene at infrared frequencies. Physical Review B, 80(24), p.245435.

[57] Zhang, Y., Tan, Y.W., Stormer, H.L. and Kim, P., 2005. Experimental observation of the quantum Hall effect and Berry's phase in graphene. Nature, 438(7065), pp.201-204.

[58] Bostwick, A., Ohta, T., Seyller, T., Horn, K. and Rotenberg, E., 2007. Quasiparticle dynamics in graphene. Nature Physics, 3(1), pp.36-40.